

Abstract

GPS radio occultation events observed between 24 July and 17 November 2008 by the IGOR occultation receiver aboard the TerraSAR-X satellite are processed and analyzed. The comparison of 16 262 refractivity profiles with collocated ECMWF data yield a mean bias of -0.60% to $+0.02\%$ at altitudes between 5 and 30 km. Standard deviations decrease from about 0.8% to 1.8% at 5 km to about 0.5% to 0.8% at about 10 km altitude. At low latitudes mean biases and standard deviations are larger, in particular in the lower troposphere. The results are consistent with 15 159 refractivity observations collected during the same time period by the BlackJack receiver aboard GRACE-A and processed by GFZ's operational processing system. The main difference between the two occultation instruments is the implementation of open-loop signal tracking in the IGOR (TerraSAR-X) receiver which improves the tropospheric penetration depth in terms of ray height by about 2 km compared to the conventional closed-loop data acquired by BlackJack (GRACE-A).

1 Introduction

On 15 June 2007 the radar satellite TerraSAR-X (4.9 m in height, 2.4 m in diameter, 1230 kg total mass and a payload mass of about 394 kg) was launched with a Russian Dnepr-1 rocket from Baikonur Cosmodrome, Kazakhstan and successfully injected into a sun-synchronous low-Earth orbit at an altitude of about 514 km and about 97.4° inclination (Werninghaus and Buckreuss, 2010). Having successfully completed its commissioning phase TerraSAR-X reached operational status on 7 January 2008; its design life time is 5 years.

TerraSAR-X's primary payload is a X-band synthetic aperture radar providing images of the Earth's surface with a maximum geometric resolution of about one meter (Pitz and Miller, 2010). In addition, the spacecraft is equipped with a laser communication instrument and the Tracking, Occultation and Ranging (TOR) experiment (Rothacher

ACPD

10, 28821–28857, 2010

Radio occultation aboard TerraSAR-X

G. Beyerle et al.

Title Page

Abstract

Introduction

Conclusions

References

Tables

Figures

◀

▶

◀

▶

Back

Close

Full Screen / Esc

Printer-friendly Version

Interactive Discussion



et al., 2007). TOR consists of a retroreflector array for satellite laser ranging measurements and the geodetic-grade Integrated GPS Occultation Receiver (IGOR). IGOR's dual-frequency carrier phase observations are used to derive the spacecraft's precise orbit with centimeter precision. Furthermore, IGOR performs GPS radio occultation (GPSRO) observations through dedicated antenna arrays mounted at the bow and stern of the spacecraft. In the following we describe the first analysis results obtained from IGOR's GPSRO measurements.

In GPSRO measurement mode signals transmitted by GPS satellites setting beyond or rising above the horizon are recorded with high sampling frequencies (Yunck et al., 2000; Kursinski et al., 1997). The signals' propagation through the ionosphere and neutral atmosphere causes characteristic changes in carrier phase and signal-to-noise ratio (SNR) which allow for the characterization of electron densities and sporadic E occurrences in the ionosphere (Hajj and Romans, 1998; Heise et al., 2002; Arras et al., 2008) and the derivation of refractivity and (dry) temperature profiles at altitudes below about 35 to 40 km (Kursinski et al., 1997). Figure 5 illustrates the GPSRO geometry schematically and defines the line-of-sight altitude (LSA). We note, that the base points (tangent point projected on Earth's surface) corresponding to LSA altitude z_{LSA} and altitude z in general deviate from each other.

Using the hydrostatic equation and the ideal gas law, vertical profiles of atmospheric refractivity are transformed into dry temperature and pressure profiles (Kursinski et al., 1997; Wickert et al., 2004). With auxiliary temperature data from meteorological analyses lower tropospheric humidity profiles are extracted from the GPSRO measurements as well (Gorbunov et al., 1996; Heise et al., 2005). GPSRO data is being used by a growing number of research groups world-wide and is considered a valuable data source for numerical weather predictions (see, e.g., Kuo et al., 2000; Anthes et al., 2008; Healy, 2008; Rennie, 2010), atmospherical physics research (see, e.g., Schmidt et al., 2008; Randel et al., 2003) and climate change studies (see, e.g., Ringer and Healy, 2008; Foelsche et al., 2008; Steiner et al., 2009; Schmidt et al., 2010).

**Radio occultation
aboard TerraSAR-X**

G. Beyerle et al.

[Title Page](#)[Abstract](#)[Introduction](#)[Conclusions](#)[References](#)[Tables](#)[Figures](#)[◀](#)[▶](#)[◀](#)[▶](#)[Back](#)[Close](#)[Full Screen / Esc](#)[Printer-friendly Version](#)[Interactive Discussion](#)

satellites independently. A maximum of 36 channels (three signal modulations from 12 satellites) are assigned to POD and up to 12 channels (three signal modulations from 4 satellites) are available to occultation measurements. The receiver firmware is implemented in a modular way, individual components may be modified during the mission by firmware uploads.

During each occultation event IGOR aboard TerraSAR-X tracks a reference signal, selected from those GPS satellites appearing at high elevation angles, simultaneously with the signal from the occulting satellite. The reference signal is used to correct for the effects of receiver clock errors. Both signals, the occulting as well as the reference signal, are recorded at a sampling rate of about 50 Hz; for technical reasons, however, the precise measurement epochs of the occulting and reference signal samples may deviate by up to 10 ms (see discussion below).

On the other hand, the IGOR instrument and its firmware differs from BlackJack deployed aboard CHAMP and GRACE in several respects. First, on TerraSAR-X occultation signals are recorded by phased-array GPS antennas which offer a higher gain in the azimuthal plane compared to the helix-type antennas used aboard CHAMP (see Sect. 4.1). As a consequence the occultation antennas' field of view is vertically restricted and the reference signal (arriving at elevation angles between about 20° and 90°) is recorded solely with the zenith antenna mounted on top of the spacecraft. Second, due to the enhanced X-band noise levels during SAR operations the general IGOR radio frequency design had to be modified for the TerraSAR-X mission. Narrow-band filter and preamplifier units were developed in order to efficiently suppress the X-band signals. These filter units are mounted on top of the receiver housing and close to the occultation antennas, respectively. Third, the IGOR instrument is driven by a temperature stabilized quartz clock which is adjusted at regular intervals to keep the GPS receiver clock time error below 1 μs with respect to GPS coordinate time. Unlike the BlackJack (CHAMP) instrument, however, the IGOR firmware suppresses these receiver clock adjustments during occultation events. Finally, the firmware currently loaded on the IGOR receiver supports open-loop C/A code signal tracking at low

**Radio occultation
aboard TerraSAR-X**

G. Beyerle et al.

Title Page

Abstract

Introduction

Conclusions

References

Tables

Figures

◀

▶

◀

▶

Back

Close

Full Screen / Esc

Printer-friendly Version

Interactive Discussion



ray tangent point altitudes to counteract the premature loss of signal lock in the lower troposphere (see, e.g., Sokolovskiy, 2001; Sokolovskiy et al., 2006, 2007; Ao et al., 2009).

3 Measurements and data analysis

5 First GPSRO measurements with IGOR (TerraSAR-X) were conducted during three brief intervals in 2007 (on 27 June, on 27 July and from 19 to 23 November 2007). A longer campaign, lasting for 32 days, was performed between 15 January and 15 February 2008. Starting on 24 July 2008 occultation events were recorded on a continuous basis until 17 November 2008. In mid-February 2009 the IGOR receiver
10 firmware was updated and occultation measurement mode was re-started on 17 February 2009. The following analysis and discussion focusses on observations recorded on 149 days between 24 July and 17 November 2008. With the exception of one week time period in early April 2010 only setting occultation events have been observed by IGOR (TerraSAR-X).

15 In a setting occultation event IGOR acquires dual frequency GPS data at an LSA of about 120 km and monitors the data in standard closed-loop (CL) tracking mode; at about -15 km LSA the C/A code channel transitions to open-loop (OL) tracking mode to avoid premature signal tracking loss in the lower troposphere (Sokolovskiy, 2001; Ao et al., 2009). OL tracking was implemented and is being successfully used by IGOR receivers aboard the COSMIC satellites (Anthes et al., 2008) as well as by the GRAS receiver aboard MetOp-A (in GRAS parlance termed 'raw sampling' tracking) (von Engeln et al., 2009). We note that IGOR's P code tracking of the L2 signal is restricted to CL operation; once the receiver transitions to OL mode, L2 carrier phase data are no longer available. Data recording of the IGOR (TerraSAR-X) ends at LSAs
20 between -90 and -150 km, typically. A histogram distribution of start, transition and end altitudes is shown in Fig. 2.

Radio occultation aboard TerraSAR-X

G. Beyerle et al.

Title Page

Abstract

Introduction

Conclusions

References

Tables

Figures



Back

Close

Full Screen / Esc

Printer-friendly Version

Interactive Discussion



Radio occultation aboard TerraSAR-X

G. Beyerle et al.

Title Page

Abstract

Introduction

Conclusions

References

Tables

Figures

◀

▶

◀

▶

Back

Close

Full Screen / Esc

Printer-friendly Version

Interactive Discussion



GPSRO observations are analyzed in three consecutive steps. First, IGOR raw data packets are extracted from the GPS data stream and individual occultation events are identified. The corresponding time-tagged carrier phase and SNR data from the occulting and the referencing satellite acquired during each occultation event (lasting for about 100 to 150 s, typically) are collected and stored in separate data files. In the next processing step carrier phase changes caused by clock drifts and the relative motion between transmitter and receiver are determined using POD information on the GPS and the TerraSAR-X spacecrafts. The POD data files, which are provided operationally by GFZ's precise orbit determination group (König et al., 2005; Michalak and König, 2010a,b), contain these estimates of positions, velocities and clock errors with a temporal resolution of 30 s. The POD data are interpolated on the occultation measurement epochs and the corresponding carrier phase contributions are calculated. In addition, the phase data are corrected for relativistic and time-of-flight effects, antenna phase center offsets and carrier phase wind-up (Kursinski et al., 1997; Hajj et al., 2002; Wickert et al., 2009; Wu et al., 1993; Beyerle, 2009) and a single differencing scheme is employed to extract excess phase path profiles (Wickert et al., 2002).

Finally, the excess phase paths are transformed into vertical profiles of bending angle and Abel-inverted to atmospheric refractivity. The processing steps from excess phase paths to bending angle, refractivity and dry temperature profiles are described by Kursinski et al. (1997); Wickert et al. (2004); Gorbunov and Lauritsen (2004); Jensen et al. (2004); the processing algorithms leading from raw data to excess phase path profiles have been discussed by Hajj et al. (2002). TerraSAR-X GPSRO results, described and discussed in the following, are derived with GFZ's experimental GPSRO processing system POCS-X.

Unlike the BlackJack (CHAMP, GRACE-A/B) receivers, IGOR (TerraSAR-X) outputs in-phase (quadrature-phase) correlation sum samples $\tilde{I}_n \equiv I_n/D_n$ ($\tilde{Q}_n \equiv Q_n/D_n$) of the occulting signal. (The reference link data packets lack the correlation sum samples.) Here, $D_n = \pm 1$ denotes the navigation data bit (see below) and I_n (Q_n) the demodulated in-phase (quadrature-phase) correlation sum for sample number n . In closed-loop

tracking mode total carrier phase samples φ_n are transmitted by IGOR; in open-loop mode, however, the receiver sends numerically-controlled oscillator (NCO) phase samples φ_n^{NCO} instead of φ_n and the total carrier phase φ_n needs to be reconstructed from φ_n^{NCO} and the residual phase samples φ_n^{res}

$$5 \quad \varphi_n = \varphi_n^{\text{NCO}} + \varphi_n^{\text{res}}, \quad (1)$$

where

$$\varphi_n^{\text{res}} = \text{atan2}(Q_n, I_n) + C_n. \quad (2)$$

The phase unwrapping term C_n is calculated from

$$C_n = \begin{cases} C_{n-1} + 2\pi & : \text{atan2}(Q_n, I_n) - \text{atan2}(Q_{n-1}, I_{n-1}) < -\pi \\ C_{n-1} - 2\pi & : \text{atan2}(Q_n, I_n) - \text{atan2}(Q_{n-1}, I_{n-1}) > +\pi \\ C_{n-1} & : \text{else} \end{cases} \quad (3)$$

10 with $C_1 = 0$ and $\text{atan2}()$ denoting the four-quadrant inverse tangent (Beyerle et al., 2006). Eqn. 3 corrects a sign error in equation (16) of Beyerle et al. (2006).

The transition between CL and OL tracking mode in terms of (demodulated) in-phase and quadrature-phase correlation sums is illustrated in Fig. 3. It shows I_n and Q_n samples as a function of LSA (top panel). Occultation event number 0502 (occulting satellite PRN 24) starts on 7 August 2008, 5 h:02 min (GPS time) at an LSA of +104.9 km and ends at an LSA of -105.6 km; at about -17.2 km LSA the receiver switches from CL to OL tracking.

15 Since the true atmospheric state is unknown a-priori, the OL Doppler model differs from the true Doppler by a few Hz and the correlation sums I and Q start to oscillate, once OL mode is active (Ao et al., 2009). The bottom panel in Fig. 3 shows the derivative of NCO phase φ_n^{NCO} with respect to time (i.e. NCO frequency) as a function of LSA. (Since in CL tracking mode the IGOR output lacks information on the NCO carrier phases, the CL φ_n^{NCO} samples are estimated from the CL φ_n^{res} using Eqn. 1 and

**Radio occultation
aboard TerraSAR-X**

G. Beyerle et al.

Title Page

Abstract

Introduction

Conclusions

References

Tables

Figures

◀

▶

◀

▶

Back

Close

Full Screen / Esc

Printer-friendly Version

Interactive Discussion



Discussion Paper | Discussion Paper | Discussion Paper | Discussion Paper

2.) The noise of φ_n^{NCO} in CL mode is determined by the bandwidth of carrier tracking loop (see, e.g., Misra and Enge, 2006). Once IGOR switches to OL mode, the carrier NCO is controlled by the Doppler model and the phase noise disappears. The step-like feature at -19.5 km LSA is caused by an adjustment of the Doppler model. These adjustments occur at integer seconds receiver time since the onboard navigation solution (which affect the OL Doppler frequency shifts) is updated once per second (for details see Ao et al., 2009). We note that during one second the (upper tropospheric or stratospheric) altitude changes by about 2 km.

Information on the tracking state is transmitted by IGOR as part of high-rate (50 Hz) raw data packets, which comprise phase and amplitude samples collected during 1 s (receiver time). I.e. the tracking state's temporal resolution is about 1 Hz and each packet contains between 49 and 51 samples. The tracking state corresponding to each individual measurement sample, however, is not encoded in the raw data stream. The following analysis is based on the assumption that tracking state transitions are aligned to the raw data packet boundaries. The switch from the CL to the OL tracking state is indicated in Fig. 3 by a color change from blue to red. Inspection of the top and bottom panel in Fig. 3 suggests, that the assumption regarding the alignment of OL-to-CL tracking state transitions might not strictly be true. It appears that the data packet starting at about -17.2 km LSA (and ending at about -19.6 km LSA) contains about 4 CL samples before the switch to OL mode occurs at about -17.4 km LSA.

Equation (2) requires knowledge of the navigation data bits D_n of the occulting satellite at the time of observation. For this purpose GFZ established a network of ground-based GPS receivers to monitor the navigation data bit stream (Beyerle et al., 2009). During the time period considered here, six out of 27 receivers within GFZ's ground-station network provided a data stream of D_n producing a global coverage of about 95%. I.e. on average about 5% of the occultation events could not be processed due to missing D_n . "Internal" navigation bit determination (Sokolovskiy et al., 2009) is not used by the POCS-X GPSRO processing system.

**Radio occultation
aboard TerraSAR-X**

G. Beyerle et al.

Title Page

Abstract

Introduction

Conclusions

References

Tables

Figures

◀

▶

◀

▶

Back

Close

Full Screen / Esc

Printer-friendly Version

Interactive Discussion



TerraSAR-X phase paths profiles are calculated using single differencing to correct for receiver clock errors (Wickert et al., 2002; Hajj et al., 2002). Two alternative methods, zero differencing and single differencing with reduced reference link sampling rate (“reduced single differencing”), are investigated as well (see following section).

As noted above, IGOR (TerraSAR-X) outputs the occultation link’s carrier phase data in terms of two separate quantities, the NCO carrier phase and the in-phase/quadrature-phase correlation sum samples not only in the OL, but also in the CL tracking state. In the latter case the “internal” navigation bits may be extracted from the in-phase correlation samples using $\tilde{D}_n \equiv s/|I_n|$ with an over-all sign factor $s = +1$ or $s = -1$. ($|x|$ denotes the modulus of x .) Since the observed (“external”) navigation bits D_n should agree with the “internal” \tilde{D}_n , provided sufficient SNR is available for the carrier phase-locked loop to track the signal without (half-)cycle slips, any differences between \tilde{D}_n and D_n can be utilized to validate the proper performance of the carrier tracking loop in CL mode. In fact, an analysis of 20 833 observations exhibits differences in 7235 cases (34.7%), in 3580 cases (17.2%) more than 50 occurrences of deviating navigation data bits are found. Inspection shows that these bit deviations occur predominantly if (C/A code) SNR values are below 50 to 100 V/V or if these SNR values exhibit strong fluctuations.

First GPSRO measurements with IGOR (TerraSAR-X) were conducted during three brief intervals in 2007 (on 27 June, on 27 July and from 19 to 23 November 2007). A longer campaign, lasting for 32 days, was performed between 15 January and 15 February 2008. Starting on 24 July 2008 occultation events were recorded on a continuous basis until 17 November 2008. In mid-February 2009 the IGOR receiver firmware was updated and occultation measurement mode was re-started on 17 February 2009. The following analysis and discussion focusses on observations recorded on 149 days between 24 July and 17 November 2008. With the exception of a one week time period in early April 2010 only setting occultation events have been observed by IGOR (TerraSAR-X).

**Radio occultation
aboard TerraSAR-X**

G. Beyerle et al.

Title Page

Abstract

Introduction

Conclusions

References

Tables

Figures

◀

▶

◀

▶

Back

Close

Full Screen / Esc

Printer-friendly Version

Interactive Discussion



4 Discussion

This section addresses four topics: first, the TerraSAR-X occultation antenna's gain pattern is compared to the helix antenna's pattern used onboard CHAMP and GRACE; second, alternatives to the standard single differencing method are investigated; third, the TerraSAR-X GPSRO refractivity observations are validated with collocated European Centre for Medium-Range Weather Forecasts (ECMWF) data and compared to GRACE-A observations recorded during the same time period.

The study is based on the analysis of setting occultation events recorded between 24 July 2008 and 17 November 2008. Starting from a data set of 20 833 excess phase path profiles recorded between 24 July 2008 and 17 November 2008 a total of 16 291 refractivity profiles are derived. Table 1 provides information on the statistics of the first and second processing stage.

4.1 Antenna gain pattern

To the best of our knowledge, laboratory calibration data of the TOR occultation antenna array's gain functions are not available. Nevertheless the gain pattern's qualitative shape can still be determined from the observed signal strengths. Fig. 4 shows the C/A code SNR values at about 40 km LSA as a function of azimuth angle derived from IGOR (TerraSAR-X) and BlackJack (CHAMP) observations within the same 21 day time period of 7 to 27 August 2008. In addition, the theoretically expected gain function, adjusted to the IGOR data by linear regression, is shown as well (green line).

The comparison of the IGOR SNR values (marked in red) with the CHAMP data (marked in blue) illustrate the improved gain pattern of the TerraSAR-X antenna array in particular at azimuth angles larger than $+20^\circ$ and smaller than -20° . As a consequence of the array design the TOR occultation antenna exhibits a narrower field of view in the vertical direction (not shown) and, thus, the reference link data cannot be recorded through the occultation antenna, but has to be observed via the zenith-oriented antenna. For comparison, in about 70% of CHAMP occultation events the

Title Page

Abstract

Introduction

Conclusions

References

Tables

Figures

◀

▶

◀

▶

Back

Close

Full Screen / Esc

Printer-friendly Version

Interactive Discussion



reference signal is observed with the occultation (helix) antenna which has similar gain patterns in the vertical and horizontal (azimuthal) direction. The data in Fig. 4 indicate a slight left-right asymmetry of IGOR's antenna gain pattern which most likely is related to the antenna's off-axis mounting position aboard TerraSAR-X.

5 4.2 Single versus zero differencing

As mentioned above (see Sect. 2), in GPSRO measurement mode IGOR tracks a reference signal from a suitably selected GPS satellite at about 50 Hz sampling rate in parallel to the occulting satellite's signal. In a single differencing retrieval the reference signal is used to eliminate excess phase deviations caused by the receiver clock errors (Wickert et al., 2002). Single differencing, however, comes at the price of a significant increase in transmitted raw data volume compared to observations without reference link data. (The increase is about 60% and less than a factor of two, because the reference link data usually include C/A and P2 carrier phases only, SNR data are not recorded.)

Since the IGOR (TerraSAR-X) firmware features suppression of receiver clock adjustments during GPSRO measurement mode (see section 2), the question arises whether the present data set could be analyzed in zero differencing mode as well. To this end the IGOR (TerraSAR-X) observations recorded between 27 July and 17 November 2008 are processed without utilization of the reference link observations. Instead, IGOR's receiver clock biases are estimated by linear interpolation of the 30 s POD solutions. The comparison of the zero differencing results in terms of the fractional refractivity error $\Delta N^{\text{ZD}}(z)/N^{\text{ECMWF}}(z)$ with

$$\Delta N^X(z) \equiv N^X(z) - N^{\text{ECMWF}}(z) \quad (4)$$

where $X = \text{ZD}$ (zero differencing), SD (single differencing), RRS (reduced rate single differencing) or NCO. N^{ZD} denotes the zero differencing refractivity and the mean and standard deviation of its fractional deviation from $N^{\text{ECMWF}}(z)$ is plotted in Fig. 5 as grey

Radio occultation aboard TerraSAR-X

G. Beyerle et al.

Title Page

Abstract

Introduction

Conclusions

References

Tables

Figures

◀

▶

◀

▶

Back

Close

Full Screen / Esc

Printer-friendly Version

Interactive Discussion



lines. $N^{\text{ECMWF}}(z)$ is the corresponding refractivity value extracted from the ECMWF meteorological field.

Another option for lowering the raw data transmission bandwidth is sampling rate reduction on the reference link. We simulate this approach (in the following denoted as reduced rate single differencing) by downsampling the reference link C/A and P2 data from 50 Hz to 1 Hz. Next, the 1 Hz data are upsampled again by linear interpolation and processed using the single differencing algorithm. The results are included in Fig. 5 as well; the comparison between derived refractivities and corresponding ECMWF analysis data in terms of the mean and standard deviation of the fraction refractivity error are plotted as black lines.

The comparison between ZD and RRSD results in Fig. 5 exhibits significant biases and enhanced standard deviations of $\Delta N^{\text{ZD}}(z)/N^{\text{ECMWF}}(z)$ starting already in the lower troposphere in comparison to the corresponding RRSD results derived from $\Delta N^{\text{RRSD}}(z)/N^{\text{ECMWF}}(z)$. The good agreement between the RRSD results (black lines in Fig. 5) and the SD results (Fig. 10 below) suggests that GPSRO raw data bandwidth could be reduced by about 60% by sampling the reference link at 1 Hz without significant loss of accuracy and precision. Second, the ZD results shown here refute the assertion by Beyerle et al. (2005) who suggested that without internal clock adjustments zero differencing processing results of observations recorded by receivers without ultra stable oscillator support were comparable to single differencing results. Rather, with presently available 30 s POD solutions zero differencing requires the presence of an ultra stable oscillator clock driving the GPSRO receiver.

4.3 Open-loop tracking

As noted above, IGOR transitions to OL tracking mode at an LSA of about -15 km (see Fig. 2). As a consequence the carrier NCO's Doppler frequency

$$f^{\text{NCO}} = \frac{d\varphi^{\text{NCO}}}{d\hat{t}} \quad (5)$$

Radio occultation aboard TerraSAR-X

G. Beyerle et al.

Title Page

Abstract

Introduction

Conclusions

References

Tables

Figures

◀

▶

◀

▶

Back

Close

Full Screen / Esc

Printer-friendly Version

Interactive Discussion



deviates from the true Doppler frequency

$$f = \frac{d\varphi}{d\hat{t}}. \quad (6)$$

once the receiver transitions to OL mode (Sokolovskiy, 2001; Beyerle et al., 2006; Ao et al., 2009). Here, the time derivative is performed with respect to receiver time \hat{t} . Figure 6 illustrates this offset between OL Doppler (NCO frequency) and true Doppler frequency, where we assume that the observed Doppler frequency may be regarded as the true Doppler frequency. In the following, the time series of f^{NCO} samples is denoted as OL Doppler model.

The left panel of Fig. 6 shows the difference $f - f^{\text{NCO}}$ as a function of LSA (grey dots) observed in 557 occultation events between 7 and 9 August 2008. The mean value of $f - f^{\text{NCO}}$, averaged at each LSA level, is marked in pink; green lines delineate the $1-\sigma$ standard deviation. The right panel indicates the number of observation samples. The profile of the mean Doppler difference agrees with the difference profile determined by Ao et al. (2009) from SAC-C observations. (Inspection of Fig. 5a in Ao et al. (2009), however, suggests that OL tracking in BlackJack (SAC-C) is activated about 15 km (LSA) higher than in IGOR (TerraSAR-X).)

An OL sampling frequency of 50 Hz implies that the values of $f - f^{\text{NCO}}$ are restricted to the frequency interval $[-25 \text{ Hz}, +25 \text{ Hz}]$; frequencies exceeding this range are aliased back into the interval $[-25 \text{ Hz}, +25 \text{ Hz}]$ and distort the OL measurement. The $1-\sigma$ standard deviations are about 10 Hz, well below the 15 Hz limit estimated by (Sokolovskiy, 2001). On the other hand, assuming the frequency samples follow a Gaussian distribution, 37% of all samples exceed the $1-\sigma$ level. Only at the $3-\sigma$ level (corresponding to about 30 Hz) this fraction decreases to 5%. Thus, an OL sampling frequency of at least 80 Hz (twice the sum of 10 Hz maximum Doppler frequency bias and a $3-\sigma$ standard deviation of 30 Hz) is necessary to track 95% of the occultation events without aliasing effects. Future firmware implementations should allow for a sampling frequency increase to at least 80 Hz. These findings are consistent with re-

**Radio occultation
aboard TerraSAR-X**

G. Beyerle et al.

Title Page

Abstract

Introduction

Conclusions

References

Tables

Figures

◀

▶

◀

▶

Back

Close

Full Screen / Esc

Printer-friendly Version

Interactive Discussion



cent results from the MetOp-A GRAS GPSRO instrument (Bonnedal et al., 2010; von Engeln et al., 2009).

The BlackJack (SAC-C) receiver and the IGOR (COSMIC) receivers modify not only the carrier loop's but also the code loop's tracking algorithm if the tracking mode transitions from CL to OL. In a rising occultation event the instrument starts out in OL tracking mode and the code NCO is controlled by a range model taking into account the estimated position and clock errors of the signal transmitter and receiver. In a setting event the range offsets are obtained directly from the carrier NCO output (Ao et al., 2009). Since the IGOR (TerraSAR-X) firmware is based on the IGOR (COSMIC) implementation it is assumed that TOR utilizes the same signal tracking strategy.

This assumption is confirmed by an analysis of the excess range

$$E_n^{\text{NCO}} \equiv \rho_n^{\text{C/A}} - \frac{\lambda}{2\pi} \varphi_n^{\text{C/A,NCO}} + C^{\text{NCO}} \quad (7)$$

which is plotted in the left panel of Fig. 7. Here, $\rho_n^{\text{C/A}}$ denotes the (C/A code) pseudorange of sample n , $\varphi_n^{\text{C/A,NCO}}$ the (C/A) NCO carrier phase and λ the (L1) carrier wavelength; the offset $C^{\text{NCO}} = -(\rho_{n=1}^{\text{C/A}} - \frac{\lambda}{2\pi} \varphi_{n=1}^{\text{C/A,NCO}})$ assures $E_{n=1}^{\text{NCO}} = 0$. Similarly,

$$E_n \equiv \rho_n^{\text{C/A}} - \frac{\lambda}{2\pi} (\varphi_n^{\text{C/A,NCO}} + \varphi_n^{\text{C/A,res}}) + C \quad (8)$$

with C/A residual carrier phase $\varphi_n^{\text{C/A,res}}$ and $C = -(\rho_{n=1}^{\text{C/A}} - \frac{\lambda}{2\pi} (\varphi_{n=1}^{\text{C/A,NCO}} + \varphi_{n=1}^{\text{C/A,res}}))$ is shown in the right panel of Fig. 7.

The constant values of the E_n^{NCO} profiles during OL tracking (Fig. 7, left panel) at LSA below about -15 km confirms that the IGOR (TerraSAR-X) firmware uses the NCO carrier phase path to steer the code NCO as described by Ao et al. (2009) for the IGOR (COSMIC) and BlackJack (SAC-C) receiver firmware. We note, that occasionally discontinuities of several tens of meters occur, when IGOR switches from CL to OL tracking mode.

**Radio occultation
aboard TerraSAR-X**

G. Beyerle et al.

Title Page

Abstract

Introduction

Conclusions

References

Tables

Figures

◀

▶

◀

▶

Back

Close

Full Screen / Esc

Printer-friendly Version

Interactive Discussion



Discussion Paper | Discussion Paper | Discussion Paper | Discussion Paper | Discussion Paper

Without ionospheric dispersion the change in total (NCO plus residual) carrier phase path may serve as an approximation of the change in true atmospheric pseudorange. Thus, the observed deviations of E_n from zero (Fig. 7, right panel) indicate an average mismodelling of the OL range model by about 50 m (1/6 of a C/A code chip length).

Obviously, the deviations between f_n^{NCO} and f map from Doppler into refractivity space as well. I.e., if the residual phases φ_n^{res} (Eqn. 2) are disregarded and refractivities are reconstructed solely from the NCO phases, the corresponding refractivities, denoted by N^{NCO} , differ from N . N^{NCO} is obtained analogous to N except that the cut-off ray height is derived from the FSI amplitude belonging to N (Jensen et al., 2003; Beyerle et al., 2006).

The resulting fractional refractivity errors with respect to ECMWF, $\Delta N^{\text{NCO}}/N^{\text{ECMWF}}$, are plotted in Fig. 8 (left panel) as black lines. The solid, dashed and dashed-dotted thick lines correspond to latitudes north of 30°N, south of 30°S and latitudes between 30°S and 30°N, respectively. For comparison, the fractional refractivity errors $\Delta N^{\text{SD}}/N^{\text{ECMWF}}$ (obtained by single differencing, see discussion in section 4.4) are plotted in grey. Below altitudes of about 7 km $\Delta N^{\text{NCO}}/N^{\text{ECMWF}}$ exhibits a significant negative bias reaching a value of about -12% at low latitudes.

In theory, the observed phase data samples φ_n are independent of the chosen OL Doppler frequency model f_n^{NCO} (Sokolovskiy, 2001). I.e., a shift of f_n^{NCO} by an offset δf will cause no change in φ_n , provided the deviation between f_n^{NCO} and the true atmospheric Doppler frequency remains below the Nyquist frequency (half of the sampling frequency) of 25 Hz (Sokolovskiy, 2001). This assumption implies that the observed refractivity values N do not correlate with the NCO refractivity N^{NCO} . We argue, however, that within the TerraSAR-X GPSRO data set the observed refractivities appear to exhibit a statistical dependency on N^{NCO} for C/A code SNRs below about 25 V/V. Specifically, the difference between N and N^{NCO} is averaged over altitudes between 0 and 3 km (denoted as $\langle N \rangle - \langle N^{\text{NCO}} \rangle$) and plotted in Fig. 9 (top panel) as a function of minimum C/A code SNR value determined within this altitude range. The individual

**Radio occultation
aboard TerraSAR-X**

G. Beyerle et al.

Title Page

Abstract

Introduction

Conclusions

References

Tables

Figures

◀

▶

◀

▶

Back

Close

Full Screen / Esc

Printer-friendly Version

Interactive Discussion



data points are sorted into SNR bins spaced by 10 V/V and mean as well as standard deviations within each bin are determined. Individual data are plotted in grey, the mean and $1-\sigma$ standard deviations are marked by red circles and vertical lines, respectively. For minimum SNRs between about 25 V/V and 150 V/V (at minimum SNRs larger than 150 V/V the number of samples are too low to be significant, see Fig. 9, bottom panel) the mean value of $\langle N - N^{\text{NCO}} \rangle$ remains at or below $-20 N$ -units. Below about 25 V/V, however, N exhibits a tendency towards N^{NCO} .

With the present OL data set we cannot provide a conclusive explanation for the observed behavior; more studies are needed to decide if this observation is relevant at all and, if it is, discuss possible solutions. As a first step forward we propose to modify the IGOR firmware and implement a second OL signal tracking channel. The carrier NCOs of the two OL channels will run at different Doppler frequencies, separated by, e.g., 25 Hz. The output of both channels will be processed individually. Quality control procedures then compare the two derived carrier phase profiles and discard the observation if the two phase path profiles are found to deviate from each other.

4.4 Validation with ECMWF analyses

In this subsection the IGOR (TerraSAR-X) refractivity profiles are compared with meteorological analysis results provided by the ECMWF. Pressure and temperature values at the time and location of the corresponding GPSRO measurement are calculated from the ECMWF fields using spatial and temporal linear interpolation between grid points ($0.5^\circ \times 0.5^\circ$ horizontal resolution) and analysis fields separated by 6 h. The vertical resolution of the GPSRO refractivities profiles is 100 m; the comparison between GPSRO observation and ECMWF data, however, is performed solely on the 91 ECMWF model levels ranging from the ground up to an altitude of about 80 km with a vertical resolution decreasing from about 25 m near the surface to about 7 km at the upper model level. ECMWF refractivities are calculated from the temperature, pressure and humidity data on the corresponding model level.

Radio occultation aboard TerraSAR-X

G. Beyerle et al.

Title Page

Abstract

Introduction

Conclusions

References

Tables

Figures

◀

▶

◀

▶

Back

Close

Full Screen / Esc

Printer-friendly Version

Interactive Discussion



**Radio occultation
aboard TerraSAR-X**

G. Beyerle et al.

[Title Page](#)[Abstract](#)[Introduction](#)[Conclusions](#)[References](#)[Tables](#)[Figures](#)[◀](#)[▶](#)[◀](#)[▶](#)[Back](#)[Close](#)[Full Screen / Esc](#)[Printer-friendly Version](#)[Interactive Discussion](#)

The result of the comparison between 16 262 IGOR (TerraSAR-X) GPSRO profiles and corresponding ECMWF data in terms of the fractional refractivity error as a function of altitude is shown in Fig. 10. For 29 observed refractivity profiles no corresponding ECMWF profile was calculated. The mean and standard deviation of $\Delta N/N^{\text{ECMWF}}$, are plotted in the left and middle panel of Fig. 10 (black lines) for the three latitudinal bands 90° S to 30° S (5319 profiles), 30° S to 30° N (5272 profiles) and 30° N to 90° N (5671 profiles). The right panel shows the number of refractivity observations as a function of altitude. 32 out of 16 262 profiles (0.2%) exhibit deviations of the fractional refractivity error $|\Delta N/N^{\text{ECMWF}}| > 20\%$ within the altitude range between 5 and 30 km. The corresponding standard deviation profiles (center panel) are marked in grey, the differences with respect to the mean fractional refractivity error (left panel) are negligible.

The biases of the mean fractional refractivity error at altitudes between 5 and 30 km is within the range of -0.60 to $+0.02\%$. Standard deviations decrease from about 0.8 to 1.8% at 5 km to about 0.5 to 0.8% at about 10 km altitude, however, increase significantly in the upper stratosphere. The strong negative bias of the mean fractional refractivity error at low latitudes and altitudes below 5 km is well known from earlier GPSRO missions (Ao et al., 2003; Xie et al., 2010) and most likely related to critical refraction at and within the tropical boundary layer.

For comparison, the corresponding mean and standard deviation of the fractional refractivity error profiles from GRACE-A observations are plotted in Fig. 11 (Beyerle et al., 2005; Wickert et al., 2009). The data set, containing 15 159 GPSRO observations, was collected during the same period as the TerraSAR-X measurements (24 July to 17 November 2008) and processed by GFZ's operational processing system POCS (Wickert et al., 2009).

The comparison of both, IGOR (TerraSAR-X) and BlackJack (GRACE-A) data with ECMWF refractivities (Figs. 10 and 11) exposes a small increase in standard deviation at the tropical tropopause (about 16–18 km altitude). Most likely these features are related to inadequate ECMWF modelling of small scale structures at the tropical

tropopause level. The occurrence of enhanced standard deviations is most prominent at the tropical tropopause level, though; in both data sets standard deviations decrease by about a factor of two when comparing refractivities at the tropopause and about 4 to 6 km below that altitude.

Furthermore, the IGOR (TerraSAR-X) results exhibit a significantly larger standard deviation compared to the GRACE-A data set (center panels in Figs. 10 and 11). The discrepancy is caused by differing filter parameters implemented in the POCS-X and POCS processing systems: POCS-X uses a polynomial derivative filter of degree three and order 61 for the derivation of the geometric Doppler frequency from the observed excess phase path profiles, whereas POCS's third degree filter is of order 100. Assuming a tangent point vertical velocity of 2 km/s these filter parameters (degree three and order 61) translate into a cut-off wavelength (-3 dB point) of about 2.0 km (see, e.g., Hamming, 1989; Beyerle and McDermid, 1999). The POCS filter parameters, on the other hand, yield a cut-off wavelength of about 3.3 km. In other words, the POCS filter attenuates vertical wavelengths shorter than about 6.7 km by more than 50%. I.e., the smaller standard deviations of POCS compared to POCS-X stratospheric refractivities are caused by the larger POCS filter order, but come at the price of a significantly coarser vertical resolution.

The main difference between the IGOR and BlackJack results in the lower troposphere is due to OL signal tracking implemented in IGOR (TerraSAR-X) and modified closed-loop ("fly-wheeling") tracking implemented in BlackJack (GRACE-A) (Ao et al., 2003; Beyerle et al., 2006). OL tracking significantly improves the data yield at altitudes below about 7 km, as is evident from the comparison of the observation number profiles (right panels in Figs. 10 and 11). The improvement in tropospheric penetration gained by OL tracking is quantitatively described in terms of the 50%-altitude $z_{50\%}$, which we define as the altitude at which the normalized number of observations decreases to 50%. Specifically, the IGOR (TerraSAR-X) data set yields $z_{50\%} = 0.85$ km, 1.27 km and 0.71 km for the three latitude regions 30° N to 90° N, 30° S to 30° N and 90° S to 30° S. These depths are about 1.5 to 4 km lower than the corresponding 50%-altitudes from

**Radio occultation
aboard TerraSAR-X**

G. Beyerle et al.

Title Page

Abstract

Introduction

Conclusions

References

Tables

Figures

◀

▶

◀

▶

Back

Close

Full Screen / Esc

Printer-friendly Version

Interactive Discussion



the BlackJack (GRACE-A) data set, which are $z_{50\%} = 3.22$ km, 5.00 km and 2.06 km for the same three latitudinal zones.

5 Conclusions

Following the BlackJack occultation receivers aboard CHAMP and the GRACE twin satellites, the IGOR instrument aboard TerraSAR-X constitutes another recent addition to current spaceborne GPSRO experiments. IGOR provides continuous GPSRO observations since July 2008. Here, 16 262 refractivity profiles collected between 24 July and 17 November 2008 are analyzed and compared with collocated ECMWF analysis data. In terms of refractivity deviations from collocated ECMWF profiles we find a mean bias of less than 0.6% within the altitude range between 5 and 30 km. In contrast to the BlackJack receivers aboard CHAMP and GRACE-A/B IGOR aboard TerraSAR-X features open-loop tracking at low ray tangent point altitudes. Open-loop signal tracking significantly improves the data yield in the lower troposphere and reduces the 50%-altitude on average by about 2.6 km. Since a significant number of observations exceed Doppler frequency deviations of 20 Hz and reach the OL Nyquist frequency of 25 Hz, an increase of the open-loop sampling rate from 50 to 100 Hz should be considered for future versions of the IGOR receiver firmware.

Acknowledgements. We gratefully acknowledge the help and support by the TerraSAR-X teams at UT-CSR, GSOC/DLR and GFZ. The European Centre for Medium-Range Weather Forecasts provided meteorological analysis fields. GFZ's navigation data bit archive may be accessed through the Information System and Data Center at <http://isdc.gfz-potsdam.de>.

Radio occultation aboard TerraSAR-X

G. Beyerle et al.

Title Page

Abstract

Introduction

Conclusions

References

Tables

Figures

◀

▶

◀

▶

Back

Close

Full Screen / Esc

Printer-friendly Version

Interactive Discussion



References

- Anthes, R. A., Bernhardt, P. A., Chen, Y., Cucurull, L., Dymond, K. F., Ector, D., Healy, S. B., Ho, S.-P., Hunt, D. C., Kuo, Y.-H., Liu, H., Manning, K., McCormick, C., Meehan, T. K., Randel, W. J., Rocken, C., Schreiner, W. S., Sokolovskiy, S. V., Syndergaard, S., Thompson, D. C., Trenberth, K. E., Wee, T.-K., Yen, N. L., and Zeng, Z.: The COSMIC/FORMOSAT-3 Mission: Early Results, *B. Am. Meteorol. Soc.*, 83, 313–333, doi:10.1175/BAMS-89-3-313, 2008. 28823, 28824, 28826
- Ao, C. O., Meehan, T. K., Hajj, G. A., Mannucci, A. J., and Beyerle, G.: Lower-Troposphere Refractivity Bias in GPS Occultation Retrievals, *J. Geophys. Res.*, 108, 4577, doi:10.1029/2002JD003216, 2003. 28838, 28839
- Ao, C. O., Hajj, G. A., Meehan, T. K., Dong, D., Iijima, B. A., Mannucci, A. J., and Kursinski, E. R.: Rising and setting GPS occultations by use of open-loop tracking, *J. Geophys. Res.*, 114, D04101, doi:10.1029/2008JD010483, 2009. 28826, 28828, 28829, 28834, 28835
- Arras, C., Wickert, J., Beyerle, G., Heise, S., Schmidt, T., and Jacobi, C.: A global climatology of ionospheric irregularities derived from GPS radio occultation, *Geophys. Res. Lett.*, 35, L14809, doi:10.1029/2008GL034158, 2008. 28823
- Beyerle, G.: Carrier phase wind-up in GPS reflectometry, *GPS Solutions*, 13, 191–198, doi:10.1007/s10291-008-0112-1, 2009. 28827
- Beyerle, G. and McDermid, I. S.: Altitude range resolution of differential absorption lidar ozone profiles, *Appl. Opt.*, 38, 924–927, doi:10.1364/AO.38.000924, 1999. 28839
- Beyerle, G., Wickert, J., Schmidt, T., and Reigber, C.: GPS radio occultation with GRACE: Atmospheric profiling utilizing the zero difference technique, *Geophys. Res. Lett.*, 32, L13806, doi:10.1029/2005GL023109, 2005. 28833, 28838
- Beyerle, G., Schmidt, T., Wickert, J., Heise, S., Rothacher, M., König-Langlo, G., and Lauritsen, K. B.: Observations and simulations of receiver-induced refractivity biases in GPS radio occultation, *J. Geophys. Res.*, 111, D12101, doi:10.1029/2005JD006673, 2006. 28828, 28834, 28836, 28839
- Beyerle, G., Ramatschi, M., Galas, R., Schmidt, T., Wickert, J., and Rothacher, M.: A data archive of GPS navigation messages, *GPS Solutions*, 13, 35–41, doi:10.1007/s10291-008-0095-y, 2009. 28829
- Bonnedal, M., Christensen, J., Carlström, A., and Berg, A.: Metop-GRAS in-orbit instrument performance, *GPS Solutions*, 14, 109–120, doi:10.1007/s10291-009-0142-3, 2010. 28835

Radio occultation aboard TerraSAR-X

G. Beyerle et al.

Title Page

Abstract

Introduction

Conclusions

References

Tables

Figures

◀

▶

◀

▶

Back

Close

Full Screen / Esc

Printer-friendly Version

Interactive Discussion



**Radio occultation
aboard TerraSAR-X**

G. Beyerle et al.

Title Page

Abstract

Introduction

Conclusions

References

Tables

Figures

◀

▶

◀

▶

Back

Close

Full Screen / Esc

Printer-friendly Version

Interactive Discussion



Foelsche, U., Borsche, M., Steiner, A. K., Gobiet, A., Pirscher, B., Kirchengast, G., Wickert, J., and Schmidt, T.: Observing upper troposphere-lower stratosphere climate with radio occultation data from the CHAMP satellite, *Clim. Dynam.*, 31, 49–65, doi:10.1007/s00382-007-0337-7, 2008. 28823

5 Gorbunov, M. E. and Lauritsen, K. B.: Analysis of wave fields by Fourier integral operators and their application for radio occultations, *Radio Sci.*, 39, RS4010, doi:10.1029/2003RS002971, 2004. 28827

Gorbunov, M. E., Gurvich, A. S., and Bengtsson, L.: Advanced algorithms of inversion of GPS/MET satellite data and their application to reconstruction of temperature and humidity, Report 211, Max-Planck-Institut für Meteorologie, Germany, Hamburg, Germany, 1996. 28823

10 Hajj, G. A. and Romans, L. J.: Ionospheric electron density profiles obtained with the Global Positioning System: Results from the GPS/MET experiment, *Radio Sci.*, 33, 175–190, doi:10.1029/97RS03183, 1998. 28823

15 Hajj, G. A., Kursinski, E. R., Romans, L. J., Bertiger, W. I., and Leroy, S. S.: A technical description of atmospheric sounding by GPS occultation, *J. Atmos. Solar-Terr. Phys.*, 64, 451–469, 2002. 28824, 28827, 28830

Hamming, R. W.: *Digital filters*, Prentice Hall, Englewood Cliffs, NJ, USA, 1989. 28839

20 Healy, S. B.: Forecast impact experiment with a constellation of GPS radio occultation receivers, *Atmos. Sci. Lett.*, 9, 111–118, doi:10.1002/asl.169, 2008. 28823

Heise, S., Jakowski, N., Wehrenpfennig, A., Reigber, C., and Lühr, H.: Sounding of the top-side ionosphere/plasmasphere based on GPS measurements from CHAMP: Initial results, *Geophys. Res. Lett.*, 29, 1699, doi:10.1029/2002GL014738, 2002. 28823

25 Heise, S., Wickert, J., Beyerle, G., Schmidt, T., and Reigber, C.: Global monitoring of tropospheric water vapor with GPS radio occultation aboard CHAMP, *Adv. Space Res.*, doi:10.1016/j.asr.2005.06.066, 2005. 28823

Jensen, A. S., Lohmann, M. S., Benzon, H.-H., and Nielsen, A. S.: Full spectrum inversion of radio occultation signals, *Radio Sci.*, 38, 1040, doi:10.1029/2002RS002763, 2003. 28836

30 Jensen, A. S., Lohmann, M. S., Nielsen, A. S., and Benzon, H.-H.: Geometrical optics phase matching of radio occultation signals, *Radio Sci.*, 39, RS3009, doi:10.1029/2003RS002899, 2004. 28827

König, R., Michalak, G., Neumayer, K. H., Schmidt, R., Zhu, S. Y., Meixner, H., and Reigber, C.: Recent developments in CHAMP orbit determination at GFZ, in: *Earth Observation with*

**Radio occultation
aboard TerraSAR-X**

G. Beyerle et al.

[Title Page](#)[Abstract](#)[Introduction](#)[Conclusions](#)[References](#)[Tables](#)[Figures](#)[◀](#)[▶](#)[◀](#)[▶](#)[Back](#)[Close](#)[Full Screen / Esc](#)[Printer-friendly Version](#)[Interactive Discussion](#)

CHAMP, Results from Three Years in Orbit, Second CHAMP Science Meeting, Potsdam, 1-4 September 2003, edited by: Reigber, C., Lühr, H., Schwintzer, P., and Wickert, J., Springer, Berlin, 65–70, doi:10.1007/3-540-26800-6_10, 2005. 28827

5 Kuo, Y.-H., Sokolovskiy, S. V., Anthes, R. A., and Vandenberghe, F.: Assimilation of GPS Radio Occultation Data for Numerical Weather Prediction, *Terrestrial, Atmos. Ocean. Sci.*, 11, 157–186, 2000. 28823

Kursinski, E. R., Hajj, G. A., Schofield, J. T., Linfield, R. P., and Hardy, K. R.: Observing Earth's atmosphere with radio occultation measurements using Global Positioning System, *J. Geophys. Res.*, 19, 23429–23465, doi:10.1029/97JD01569, 1997. 28823, 28827

10 Michalak, G. and König, R.: Rapid Science Orbits for CHAMP and GRACE Radio Occultation Data Analysis, in: *System Earth via Geodetic-Geophysical Space Techniques*, edited by: Flechtner, F., Gruber, T., Guentner, A., Manda, M., Rothacher, M., Schoene, T., and Wickert, J., Springer-Verlag, Berlin, 67–77, doi:10.1007/978-3-642-10228-8_6, 2010a. 28827

15 Michalak, G. and König, R.: Near-Real Time Satellite Orbit Determination for GPS Radio Occultation with CHAMP and GRACE, in: *System Earth via Geodetic-Geophysical Space Techniques*, edited by: Flechtner, F., Gruber, T., Guentner, A., Manda, M., Rothacher, M., Schoene, T., and Wickert, J., pp. 443–454, Springer-Verlag, Berlin, Germany, doi:10.1007/978-3-642-10228-8_39, 2010b. 28827

20 Misra, P. and Enge, P.: *Global Positioning System: Signals, Measurements, and Performance*, Ganga-Jamuna Press, Lincoln, MA 01773, USA, 2006. 28829

Pitz, W. and Miller, D.: The TerraSAR-X Satellite, *IEEE Trans. Geosci. Remote Sens.*, 48, 615–622, doi:10.1109/TGRS.2009.2037432, 2010. 28822

25 Randel, W. J., Wu, F., and Ríos, W. R.: Thermal variability of the tropical tropopause region derived from GPS/MET observations, *J. Geophys. Res.*, 108, 4024, doi:10.1029/2002JD002595, 2003. 28823

Rennie, M. P.: The impact of GPS radio occultation assimilation at the Met Office, *Q. J. Roy. Meteorol. Soc.*, 136, 116–131, doi:10.1002/qj.521, 2010. 28823

30 Ringer, M. A. and Healy, S. B.: Monitoring twenty-first century climate using GPS radio occultation bending angles, *Geophys. Res. Lett.*, 35, L05708, doi:10.1029/2007GL032462, 2008. 28823

Rocken, C., Anthes, R., Exner, M., Hunt, D., Sokolovskiy, S., Ware, R., Gorbunov, M., Schreiner, W., Feng, D., Herman, B., Kuo, Y.-H., and Zou, X.: Analysis and validation of GPS/MET data in the neutral atmosphere, *J. Geophys. Res.*, 102, 29849–29866, doi:10.1029/97JD02400,

**Radio occultation
aboard TerraSAR-X**

G. Beyerle et al.

Title Page

Abstract

Introduction

Conclusions

References

Tables

Figures

◀

▶

◀

▶

Back

Close

Full Screen / Esc

Printer-friendly Version

Interactive Discussion



1997. 28824

Rothacher, M., Tapley, B. D., Reigber, C., König, R., Falck, C., Grunwaldt, L., Köhler, W., Massmann, F.-H., and Michalak, G.: The tracking, occultation and ranging (TOR) instrument onboard TerraSAR-X and TanDEM-X, in: Proc. IEEE IGARSS, 23–28 July, 2007, 4983–4986, 2007. 28822

Schmidt, T., de la Torre, A., and Wickert, J.: Global gravity wave activity in the tropopause region from CHAMP radio occultation data, *Geophys. Res. Lett.*, 35, L16807, doi:10.1029/2008GL034986, 2008. 28823

Schmidt, T., Wickert, J., and Haser, A.: Variability of the upper troposphere and lower stratosphere observed with GPS radio occultation bending angles and temperatures, *Adv. Space Res.*, 46, 150–161, doi:10.1016/j.asr.2010.01.021, 2010. 28823

Sokolovskiy, S., Rocken, C., Hunt, D., Schreiner, W., Johnson, J., Masters, D., and Esterhuizen, S.: GPS profiling of the lower troposphere from space: Inversion and demodulation of the open-loop radio occultation signals, *Geophys. Res. Lett.*, 33, L14816, doi:10.1029/2006GL026112, 2006. 28826

Sokolovskiy, S. V.: Tracking tropospheric radio occultation signals from low Earth orbit, *Radio Sci.*, 36, 483–498, doi:10.1029/1999RS002305, 2001. 28826, 28834, 28836

Sokolovskiy, S. V., Rocken, C., Lenschow, D. H., Kuo, Y.-H., Anthes, R. A., Schreiner, W. S., and Hunt, D. C.: Observing the moist troposphere with radio occultation signals from COSMIC, *Geophys. Res. Lett.*, 34, L18802, doi:10.1029/2007GL030458, 2007. 28826

Sokolovskiy, S. V., Schreiner, W. S., Rocken, C., and Hunt, D. C.: Optimal noise filtering for the ionospheric correction of GPS radio occultation signals, *J. Ocean. Atmos. Technol.*, 26, 1398–1403, doi:10.1175/2009JTECHA1192.1, 2009. 28829

Steiner, A. K., Kirchengast, G., Lackner, B. C., Pirscher, B., Borsche, M., and Foelsche, U.: Atmospheric temperature change detection with GPS radio occultation 1995 to 2008, *Geophys. Res. Lett.*, 36, L18702, doi:10.1029/2009GL039777, 2009. 28823

von Engeln, A., Healy, S., Marquardt, C., Andres, Y., and Sancho, F.: Validation of operational GRAS radio occultation data, *Geophys. Res. Lett.*, 36, L17809, doi:10.1029/2009GL039968, 2009. 28826, 28835

Werninghaus, R. and Buckreuss, S.: The TerraSAR-X Mission and System Design, *IEEE Trans. Geosci. Remote Sens.*, 48, 606–614, doi:10.1109/TGRS.2009.2031062, 2010. 28822

Wickert, J., Beyerle, G., Hajj, G. A., Schwieger, V., and Reigber, C.: GPS radio occultation with CHAMP: Atmospheric profiling utilizing the space-based single difference technique,

- Geophys. Res. Lett., 29, 1187, doi:10.1029/2001GL013982, 2002. 28827, 28830, 28832
- Wickert, J., Schmidt, T., Beyerle, G., König, R., Reigber, C., and Jakowski, N.: The radio occultation experiment aboard CHAMP: Operational data analysis and validation of atmospheric profiles, *J. Meteorol. Soc. Jpn.*, 82, 381–395, 2004. 28823, 28827
- 5 Wickert, J., Michalak, G., Schmidt, T., Beyerle, G., Cheng, C., Healy, S., Heise, S., Huang, C., Jakowski, N., Köhler, W., Mayer, C., Offiler, D., Ozawa, E., Pavelyev, A., Rothacher, M., Tapley, B., and Arras, C.: GPS radio occultation: Results from CHAMP, GRACE and FORMOSAT-3/COSMIC, *Terrestrial, Atmos. Ocean. Sci.*, 20, 35–50, doi:10.3319/TAO.2007.12.26.01(F3C), 2009. 28824, 28827, 28838
- 10 Wu, J. T., Wu, S. C., Hajj, G. A., Bertiger, W. I., and Lichten, S. M.: Effects of antenna orientation on GPS carrier phase, *Manuscripta Geodaetica*, 18, 91–98, 1993. 28827
- Xie, F., Wu, D. L., Ao, C. O., Kursinski, E. R., Mannucci, A. J., and Syndergaard, S.: Super-refraction effects on GPS radio occultation refractivity in marine boundary layers, *Geophys. Res. Lett.*, 35, L11805, doi:10.1029/2010GL043299, 2010. 28838
- 15 Yunck, T. P., Liu, C.-H., and Ware, R.: A History of GPS Sounding, *Terrestrial, Atmos. Ocean. Sci.*, 11, 1–20, 2000. 28823

**Radio occultation
aboard TerraSAR-X**

G. Beyerle et al.

Title Page

Abstract

Introduction

Conclusions

References

Tables

Figures

I◀

▶I

◀

▶

Back

Close

Full Screen / Esc

Printer-friendly Version

Interactive Discussion



Radio occultation aboard TerraSAR-X

G. Beyerle et al.

Table 1. Occultation events statistics for 39 987 raw observations recorded between 24 July and 17 November 2008. 39 987–20833 = 19154 events are removed in the first processing stage (derivation of bending angles from excess phase paths), another 20833 – 16291 = 4542 events are flagged as deficient in the second processing stage (derivation of refractivity profiles from bending angles).

occurrences	description
39 987	number of raw data observations
– 11 437	occultation event too short
– 2396	missing navigation bit data
– 1423	precise orbit information lacking
– 3898	other errors
20 833	number of remaining excess phase profiles
– 3164	ionospheric correction failed
– 710	insufficient altitude range
– 326	errors within wave optics processing (FSI)
– 342	other errors
16 291	number of remaining refractivity profiles

[Title Page](#)
[Abstract](#)
[Introduction](#)
[Conclusions](#)
[References](#)
[Tables](#)
[Figures](#)
[Back](#)
[Close](#)
[Full Screen / Esc](#)
[Printer-friendly Version](#)
[Interactive Discussion](#)


**Radio occultation
aboard TerraSAR-X**

G. Beyerle et al.

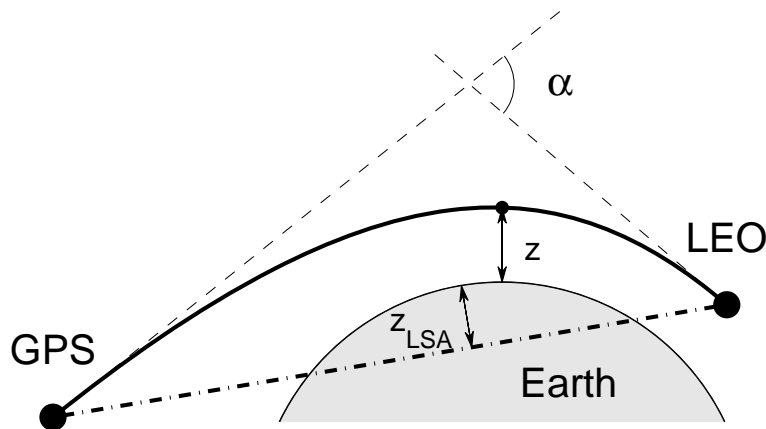


Fig. 1. Schematic diagram of the occultation geometry. Ionospheric and atmospheric refraction deflects the ray (solid line) by bending angle α . z denotes the altitude of the ray tangent point above the ellipsoid, z_{LSA} the line-of-sight (dashed-dotted) altitude. Note that in the lower troposphere z_{LSA} may become negative. (Figure is not to scale.)

[Title Page](#)[Abstract](#)[Introduction](#)[Conclusions](#)[References](#)[Tables](#)[Figures](#)[I◀](#)[▶I](#)[◀](#)[▶](#)[Back](#)[Close](#)[Full Screen / Esc](#)[Printer-friendly Version](#)[Interactive Discussion](#)

**Radio occultation
aboard TerraSAR-X**

G. Beyerle et al.

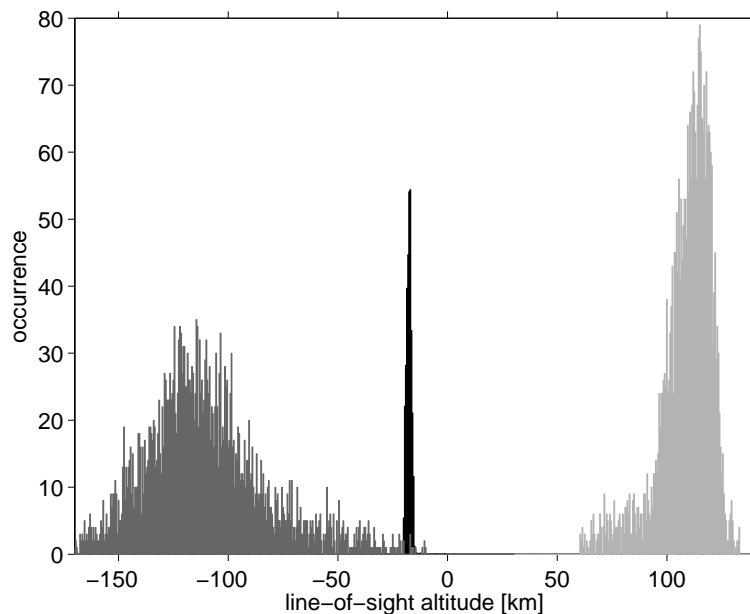


Fig. 2. Histogram distribution of line-of-sight altitudes marking the start (light grey) and end (dark grey) of occultation events; the altitudes of the transition between closed-loop and open-loop tracking is marked in black. The analysis is based on 3182 setting GPSRO events recorded between 7 and 21 August 2008. For clarity, the occurrence of the CL/OL transition heights is reduced by a factor of ten.

[Title Page](#)[Abstract](#)[Introduction](#)[Conclusions](#)[References](#)[Tables](#)[Figures](#)[◀](#)[▶](#)[◀](#)[▶](#)[Back](#)[Close](#)[Full Screen / Esc](#)[Printer-friendly Version](#)[Interactive Discussion](#)

Radio occultation
aboard TerraSAR-X

G. Beyerle et al.

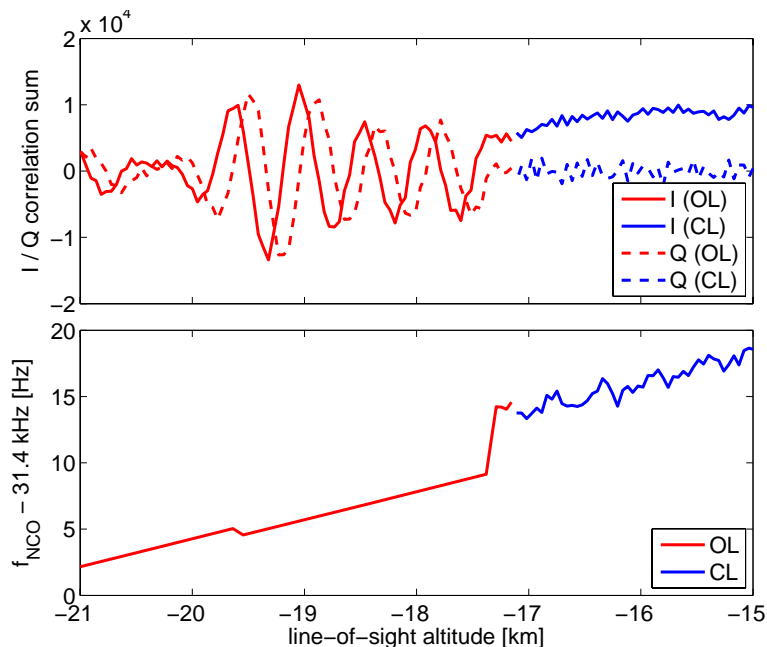


Fig. 3. Transition between closed-loop (line-of-sight altitude above -17.2 km) and open-loop mode (line-of-sight altitude below -17.2 km). Top: in-phase (solid line) and quadrature-phase (dashed line) correlation sum samples as a function of line-of-sight altitude. Samples acquired in closed-loop (open-loop) mode are plotted in blue (red). Bottom: the corresponding NCO frequency (for clarity shifted by 31.4 kHz) as a function of line-of-sight altitude. For details see text.

Title Page

Abstract

Introduction

Conclusions

References

Tables

Figures

◀

▶

◀

▶

Back

Close

Full Screen / Esc

Printer-friendly Version

Interactive Discussion



**Radio occultation
aboard TerraSAR-X**

G. Beyerle et al.

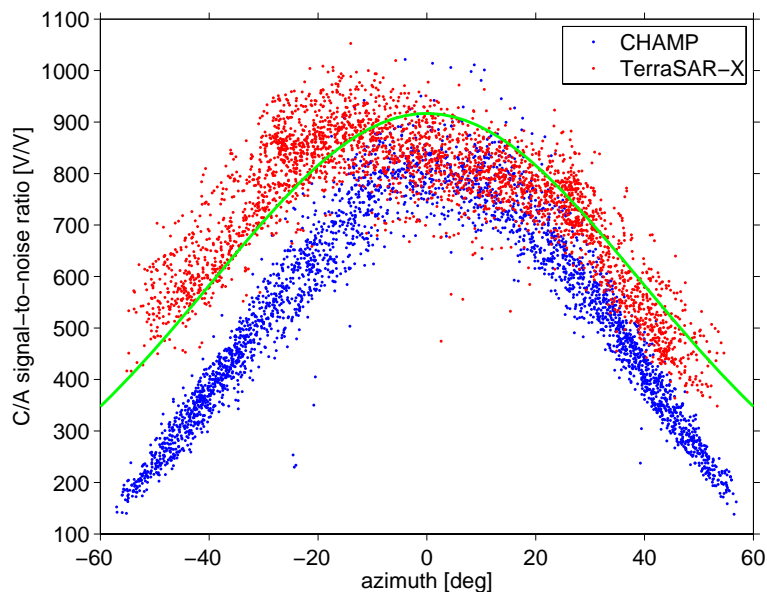


Fig. 4. C/A code SNR values at a line-of-sight altitude of 40 km versus the azimuth angle of the corresponding observation. The figure shows 3182 occultation events recorded by IGOR (TerraSAR-X) between 7 and 27 August 2008 marked in red. For comparison 3034 events recorded by BlackJack (CHAMP) during the same time period are shown (blue dots). The green line is derived from the theoretically expected occultation antenna's gain function.

[Title Page](#)[Abstract](#)[Introduction](#)[Conclusions](#)[References](#)[Tables](#)[Figures](#)[◀](#)[▶](#)[◀](#)[▶](#)[Back](#)[Close](#)[Full Screen / Esc](#)[Printer-friendly Version](#)[Interactive Discussion](#)

Radio occultation
aboard TerraSAR-X

G. Beyerle et al.

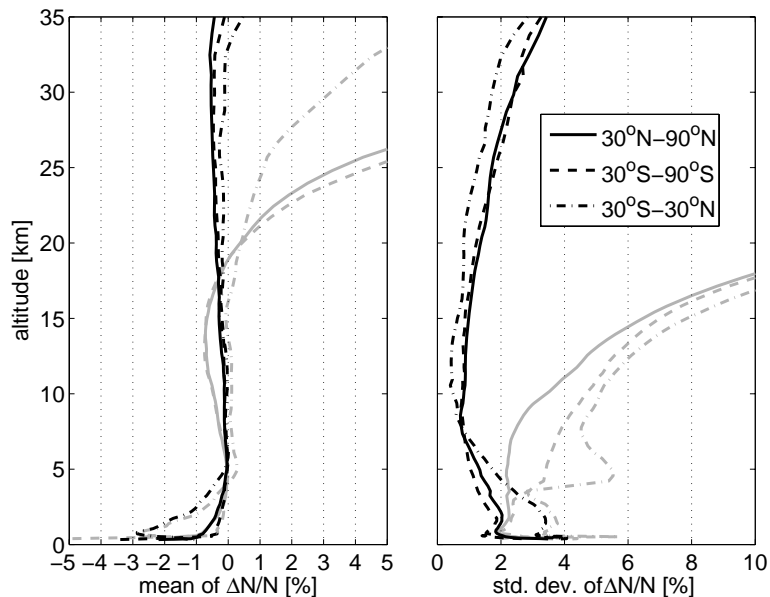


Fig. 5. Reduced rate differencing and zero differencing. Left: mean fractional refractivity error for three meridional zones; dashed line: 90°S–30°S, dashed-dotted: 30°S–30°N, solid: 30°N–90°N. The sampling frequency on the reference link is reduced to 1 Hz (black lines); the corresponding zero differencing results are drawn as grey lines. Right: standard deviation of fractional refractivity error for 1 Hz single differencing (black) and zero differencing (grey).

[Title Page](#)
[Abstract](#)
[Introduction](#)
[Conclusions](#)
[References](#)
[Tables](#)
[Figures](#)
[◀](#)
[▶](#)
[◀](#)
[▶](#)
[Back](#)
[Close](#)
[Full Screen / Esc](#)
[Printer-friendly Version](#)
[Interactive Discussion](#)


Radio occultation
aboard TerraSAR-X

G. Beyerle et al.

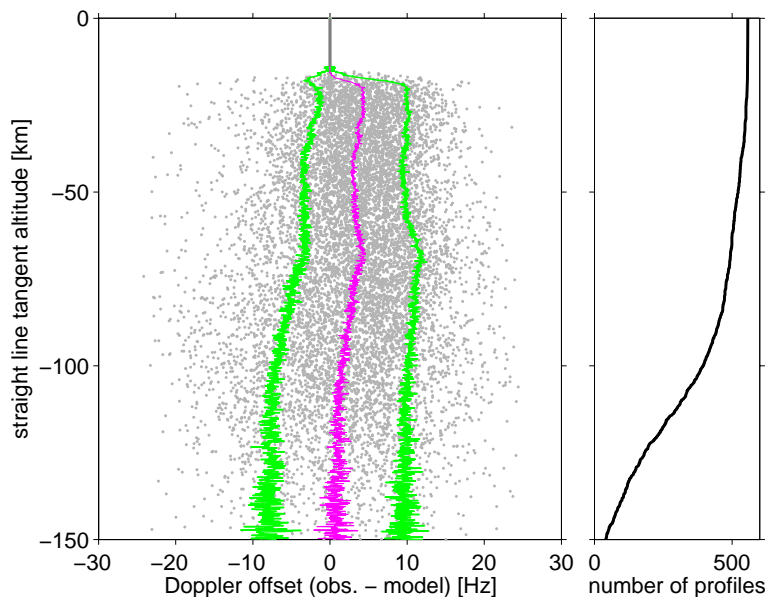


Fig. 6. Left: Difference between total and NCO frequency as a function of line-of-sight altitude. The mean and 1- σ standard deviation are plotted in pink and green, respectively; the individual data points (for clarity only 2% of the data points are shown) are marked in grey. Right: number of observation samples as a function of line-of-sight altitude. For details see text.

[Title Page](#)[Abstract](#)[Introduction](#)[Conclusions](#)[References](#)[Tables](#)[Figures](#)[◀](#)[▶](#)[◀](#)[▶](#)[Back](#)[Close](#)[Full Screen / Esc](#)[Printer-friendly Version](#)[Interactive Discussion](#)

Radio occultation
aboard TerraSAR-X

G. Beyerle et al.

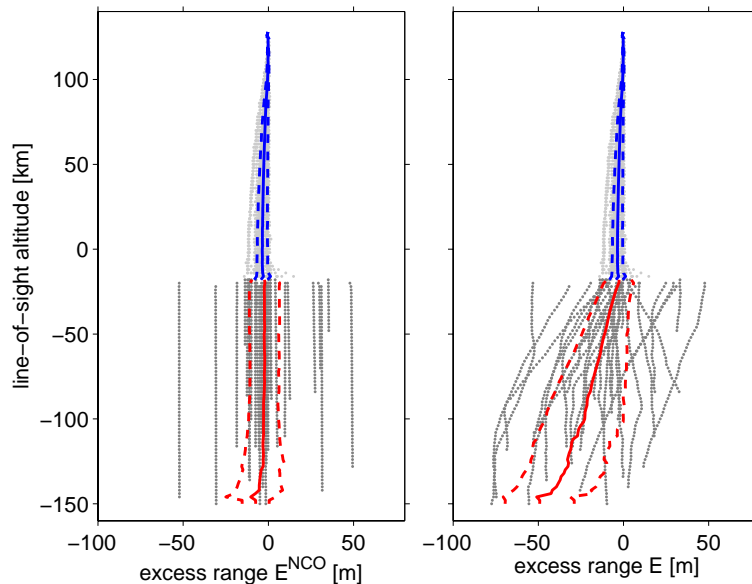


Fig. 7. Range deviation for 180 occultation events recorded on 7 August 2008. Left: excess range E^{NCO} as a function of line-of-sight altitude. Right: excess range E as a function of line-of-sight altitude. The individual closed-loop (open-loop) data points are marked in light (dark) grey. Solid and dashed lines indicate the mean and $1\text{-}\sigma$ standard deviations for the two subsets (OL in red, CL in blue). 4 events with deviations exceeding 100 m are excluded from the statistics. (For details see text.)

[Title Page](#)[Abstract](#)[Introduction](#)[Conclusions](#)[References](#)[Tables](#)[Figures](#)[◀](#)[▶](#)[◀](#)[▶](#)[Back](#)[Close](#)[Full Screen / Esc](#)[Printer-friendly Version](#)[Interactive Discussion](#)

Radio occultation
aboard TerraSAR-X

G. Beyerle et al.

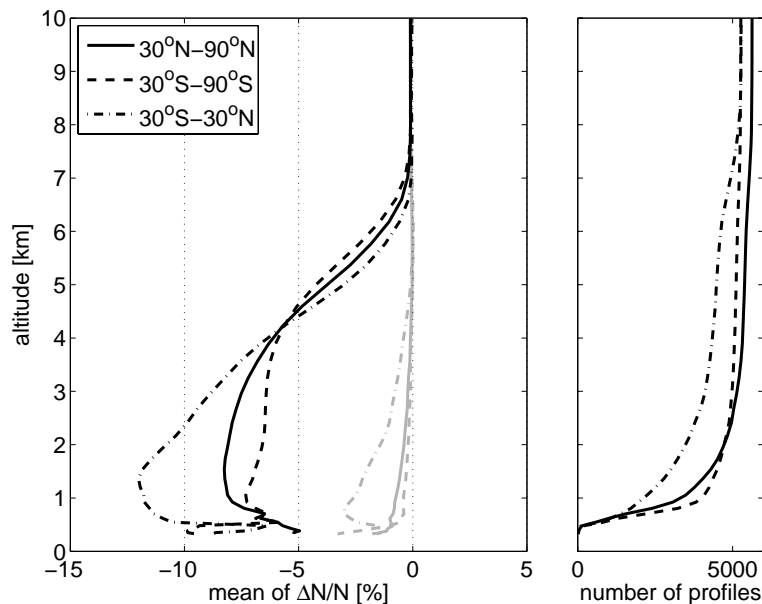


Fig. 8. Left: Fractional refractivity error derived solely from NCO phase data ignoring contributions from the residual phase samples (black lines). The results for the full measurement period (24 July and 17 November 2008) at three latitudinal bands are plotted as solid, dashed and dashed-dotted lines, respectively. For comparison the results obtained from the total (NCO plus residual) phase samples are shown as well (grey lines). Right: number of data points within the three latitudinal regions.

Title Page

Abstract

Introduction

Conclusions

References

Tables

Figures

◀

▶

◀

▶

Back

Close

Full Screen / Esc

Printer-friendly Version

Interactive Discussion



Radio occultation
aboard TerraSAR-X

G. Beyerle et al.

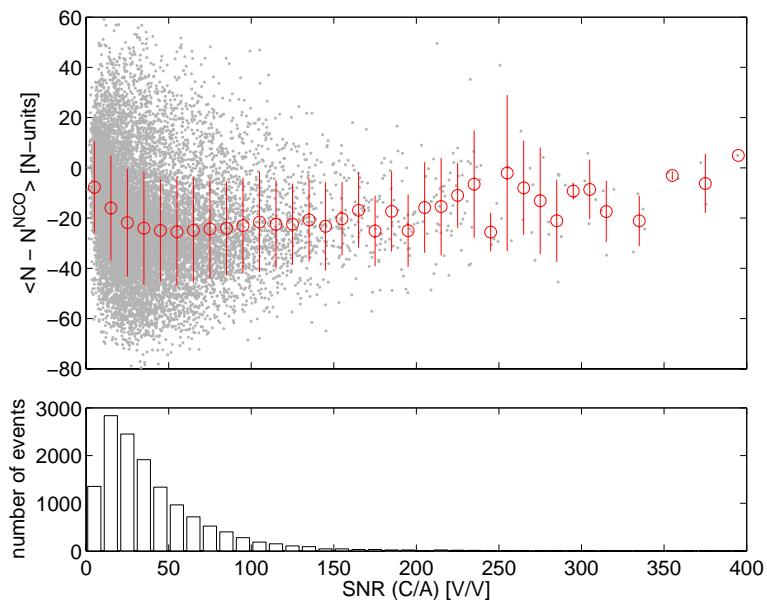


Fig. 9. Top: difference between the refractivities N and N^{NCO} , averaged between 0 and 3 km altitude, as a function of C/A code SNR (grey dots). Red circles mark the mean values in SNR bins spaced 10 V/V, vertical lines indicated the $1\text{-}\sigma$ standard deviation. The analysis is based on the complete data set obtained during the time period 24 July to 17 November 2008. Bottom: number of occultation events within the individual SNR bins. (For details see text.)

[Title Page](#)[Abstract](#)[Introduction](#)[Conclusions](#)[References](#)[Tables](#)[Figures](#)[◀](#)[▶](#)[◀](#)[▶](#)[Back](#)[Close](#)[Full Screen / Esc](#)[Printer-friendly Version](#)[Interactive Discussion](#)

Radio occultation
aboard TerraSAR-X

G. Beyerle et al.

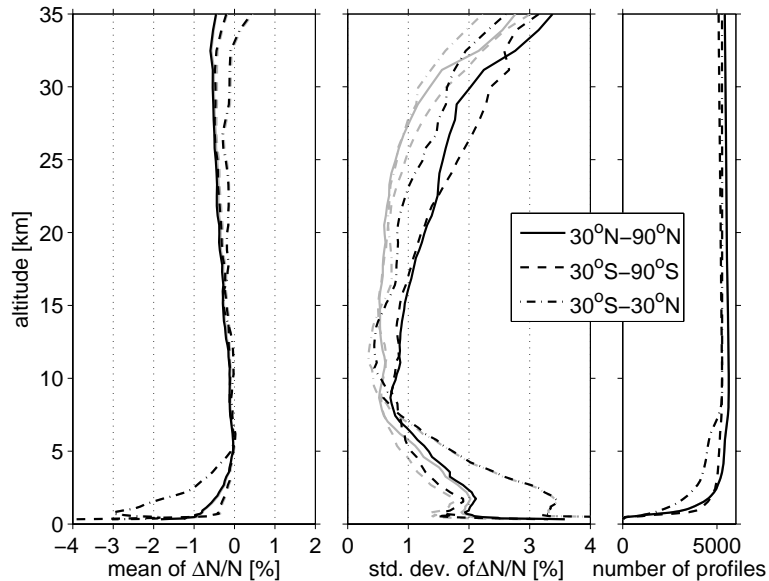


Fig. 10. Statistical comparison of 16262 IGOR (TerraSAR-X) refractivity profiles with collocated ECMWF analysis results. The observation period is 24 July to 17 November 2008. Left: mean fractional refractivity error for three meridional zones, 90° S–30° S (dashed lines), 30° S–30° N (dashed-dotted), 30° N–90° N (solid). Center: standard deviation of fractional refractivity error. Results marked in grey are obtained, if 32 observations (0.2%) deviating by more than 20% from the corresponding ECMWF profile within the altitude range of 5 to 30 km are removed from the data set. Right: number of data points. Data has been processed by GFZ's experimental processing system POCS-X.

Radio occultation
aboard TerraSAR-X

G. Beyerle et al.

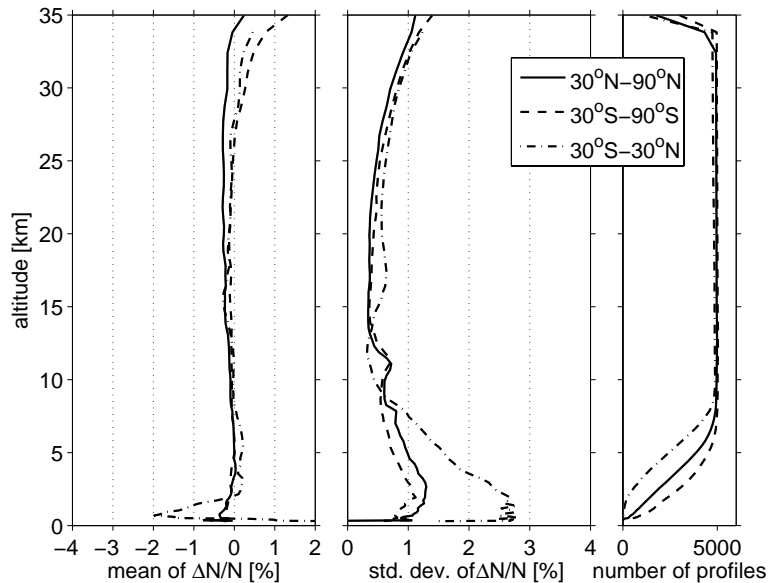


Fig. 11. Same as Fig. 10 but for 15 159 GRACE-A GPSRO observations recorded during the same time period and processed by GFZ's operational processing system POCS.

Title Page

Abstract

Introduction

Conclusions

References

Tables

Figures

◀

▶

◀

▶

Back

Close

Full Screen / Esc

Printer-friendly Version

Interactive Discussion

